Fuel Disruption Mechanisms Determined In-Pile in the ACRR

Steven A. Wright, Erhard A. Fischer

Prepared for
U. S. NUCLEAR REGULATORY COMMISSION

SF2900Q(8-81)

Available from

GPO Sal s Program
Division of Technical Information and Document Control
U.S. Nuclear Regulatory Commission
Washington, D.C. 20555

and

National Technical Information Service
Springfield, Virginia 22161

FUEL DISRUPTION MECHANISMS DETERMINED
IN-PILE IN THE ACRR

Steven A. Wright
Erhard A. Fischer

ABSTRACT

Over thirty in-pile experiments were performed to investigate fuel disruption behavior for LMFBR loss of flow (LOF) accidents. These experiments reproduced the heating transients for a variety of accidents ranging from slow LOF accidents to rapid LOF-driven-TOP accidents. In all experiments the timing and mode of the fuel disruption were observed with a high speed camera, enabling detailed comparisons with a fuel pin code, SANDPIN. This code transient intra- and inter-granular fission gas behavior to predict the macroscopic fuel behavior, such as fission gas induced swelling and frothing, cracking and breakup of solid fuel, and fuel vapor pressure driven dispersal.

This report reviews the different modes of fuel disruption as seen in the experiments and then describes the mechanism responsible for the disruption. An analysis is presented that describes a set of conditions specifying the mode of fuel disruption and the heating conditions required to produce the disruption. The heating conditions are described in terms of heating rate (K/s), temperature gradient, and fuel temperature. A fuel disruption map is presented which plots heating rate as a function of fuel temperature to illustrate the different criteria for disruption. Although this approach to describing fuel disruption oversimplifies the fission gas processes modeled by SANDPIN, it does illustrate the criteria used to determine which fuel disruption mechanism is dominant and on what major fission gas parameters it depends.

CONTENTS

ILLUSTRATIONS

TABLES

FUEL DISRUPTION MECHANISMS DETERMINED
IN-PILE IN THE ACRR

Steven A. Wright
Sandia National Laboratories
Albuquerque, NM 87185 USA

Erhard A. Fischer**
Kernforschungszentrum Karlsruhe GMBH
Karlsruhe, Germany

1.0 INTRODUCTION

The ACRR Fuel Disruption program (FD) at Sandia has investigated fuel behavior during the initiation phase of LMFBR accidents. In over 30 in-pile experiments the fuel behavior was visually observed with high speed cinematography in the Annular Core Research Reactor (ACRR). The experiments therefore provide a detailed data base to aid in the development and verification of early fuel behavior models for accident analysis. In addition, phenomenological models of fission gas mechanisms are being developed in a code called SANDPIN, to predict the time and mode of fuel disruption.

The initial disruption is important in determining the severity of reactor accidents because it affects subsequent fuel and clad relocation.[1] Some types of disruption (cracking or breakup of solid fuel) may allow more efficient sweep out of fuel, thus promoting early neutronic termination of the accident. Other disruption modes (swelling or foaming) may delay or inhibit the dispersive relocation of fuel, which increases the severity of the accident. Thus, it is important to study the disruption of fuel and cladding to determine when it occurs and its mode of disruption.

The experiments in the FD program were performed in three series, which are summarized in Table 1.1. Funding for these experiments was jointly sponsored by the US-NRC, the UKAEA, and the FRG-KfK. The first experiment series, FD1, consisted of 12 scoping experiments which proved the technique of using cinematography to provide detailed data on fuel disruption. This series scoped a range of reactor accidents including LOF and prompt burst disassembly accidents.[2] The second series investigated fuel disruption during prompt burst heating conditions.[3] These experiments were called the High Ramp Rate (HRR) experiments because of the rapid fuel heating rates (50 to 100 K/ms).

The most recent series was called the FD2/4 series. It investigated the LOF accidents representative of CRBR and SNR-300.[4],[5],[6] The CRBR has a homogeneous core design while SNR-300 has a heterogeneous design; therefore, the heating conditions differ slightly. Thus, the experiments in this series are labeled FD2 or FD4, and refer to the LOF accident scenarios for CRBR and SNR.

TABLE 1.1

Summary of the FD Program

Experiment Series	Sponsorship	Type of Experiment
FD1	USNRC	12 Scoping Experiments of LOF & Prompt Burst Accident Scenarios
HRR	USNRC,UKAEA	6 LOF-d-TOP Accident Scenarios
FD2/4	USNRC, FRG-KfK	14 LOF Accident Scenarios for CRBR and SNR-300

The experiments exhibited a spectrum of disruption modes with dispersive characters dependent on the heating rate, fission gas content, and radial temperature gradient. The observed disruption modes consisted of modest radial swelling in solid fuel (10%), sub-stantial frothing in molten fuel (4 to 6 times the original volume), sputtering, solid state cracking (accompanied by rapid radial dis-persal), and very rapid liquid fuel dispersal. This report reviews the different modes of fuel disruption as seen in the experiments and describes the mechanisms responsible for the disruption. The results can be summarized in a fuel disruption map which plots heating rate as a function of fuel temperature to illustrate the different criteria for disruption. Although this approach to describing fuel disruption oversimplifies the fission gas processes modeled by SANDPIN, it does illustrate the criteria used to determine which fuel disruption mecha-nism is dominant and on what major fission gas parameters it depends.

2.0 EXPERIMENTAL REVIEW AND RESULTS

This section summarizes the major results of the FD program and describes experimental conditions such as power histories and temperature profiles. In addition, a brief description of the fuel behavior is given. A few selected experiments are described to illustrate the different modes of fuel disruption.

Significant uncertainties exist in the predicted accident scenarios due to lack of phenomenological understanding and inaccurate knowledge of physical parameters (sodium void worth and doppler coefficient). In addition, incoherencies among subassemblies naturally occur, thus the timing and mode of disruption are not uniform in a large LMFBR. To bound disruptive fuel behavior during LOF accidents, a range of power histories must be considered.

Four major types of power histories were used in the FD program. Figure 2.1 shows the three types of power histories used in the FD2/4 series of experiments[4][5], and Figure 2.2 shows a typical power history used in the HRR series.[3] The first curve in Figure 2 illustrates the SAS-predicted LOF power history for CRBR (ACRR power history used for experiment FD2.6).[7] In this accident scenario boiling is expected to occur between six and seven seconds when the reactor power is near its nominal level. Because of the low sodium void worth (due to its heterogeneous design), the reactor power slowly increases, and eventually the clad melts and relocates, causing a more rapid increase in power level. When the power reaches 5 to 6 times nominal power, fuel melting and fuel disruption are expected to occur.

The second curve in Figure 2.1 shows the ACRR power history used to reproduce SAS-predicted LOF heating conditions for SNR-300.[8] This reactor has a higher sodium void worth than CRBR (due to SNR's homogeneous design), and in this accident scenario sodium boiling causes a more rapid rise to higher power (14-16 times nominal power). Fuel disruption is expected to occur when the fuel and clad are both partially molten. Thus, fuel disruption and relocation occur concurrently with clad relocation. As is shown later, the presence of clad significantly affects the mode of disruption.

The third power history (for experiment FD4.1) represents a bounding accident transient for either CRBR or SNR-300. This power history is essentially identical to the CRBR LOF transient (FD2.6) except that the maximum power level is twice as large (12 x P_o versus 6 x P_o). Alternatively, this power history is similar to the SNR accident scenario (FD4.3) except that the disruptive transient occurs after clad relocation.

The fourth type of power history is illustrated in Figure 2.2. The experiments using this power history simulated the heating conditions of LOF-driven-TOP accidents rather that LOF accidents. Consequently, the heating rates were much higher, on the order of 50,000 to 100,000 K/s (180-340 x P_o) rather than the 700 to 4,000 K/s (6-16 x P_o) heating rates used in the FD2/4 series. The first pulse was used
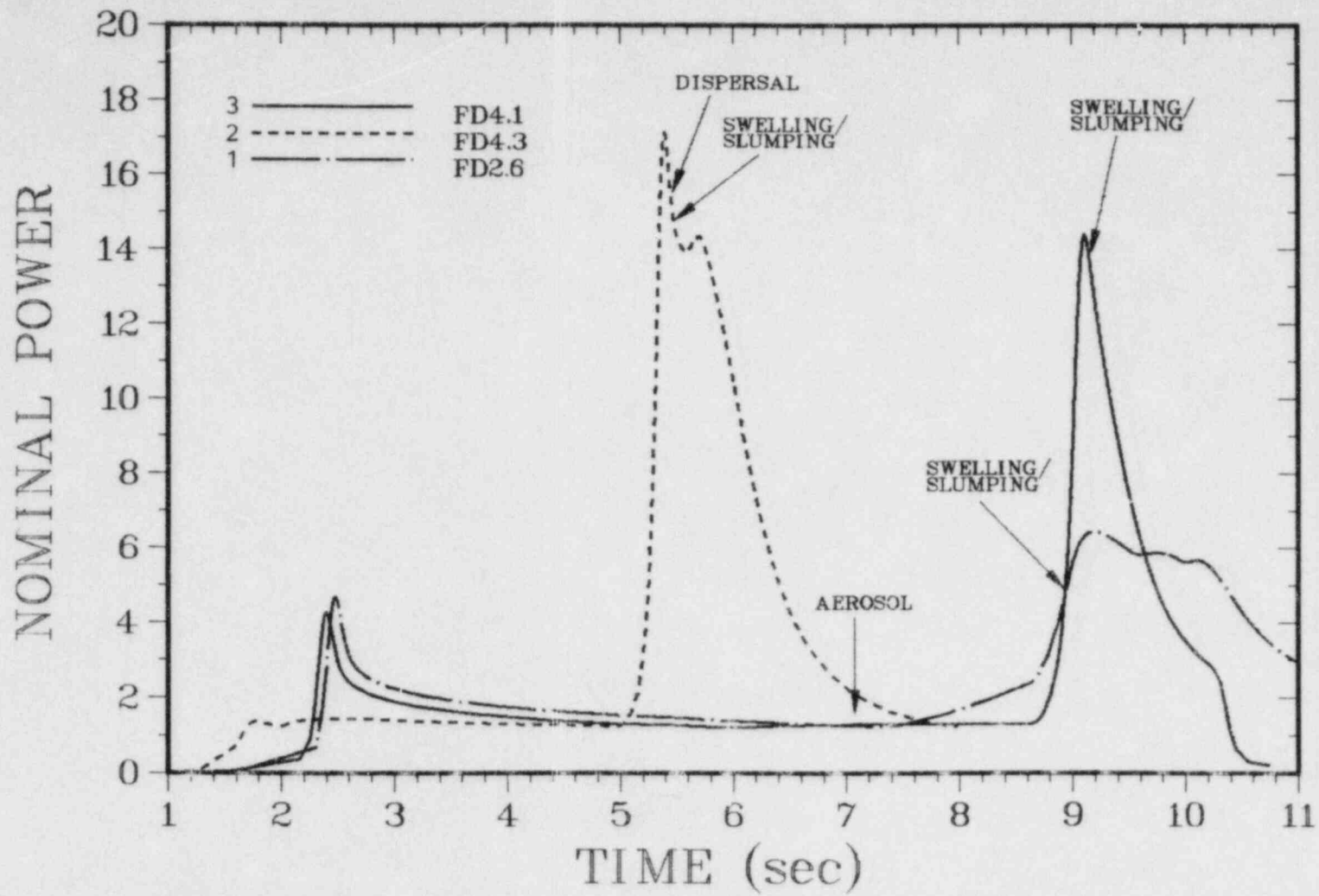
3

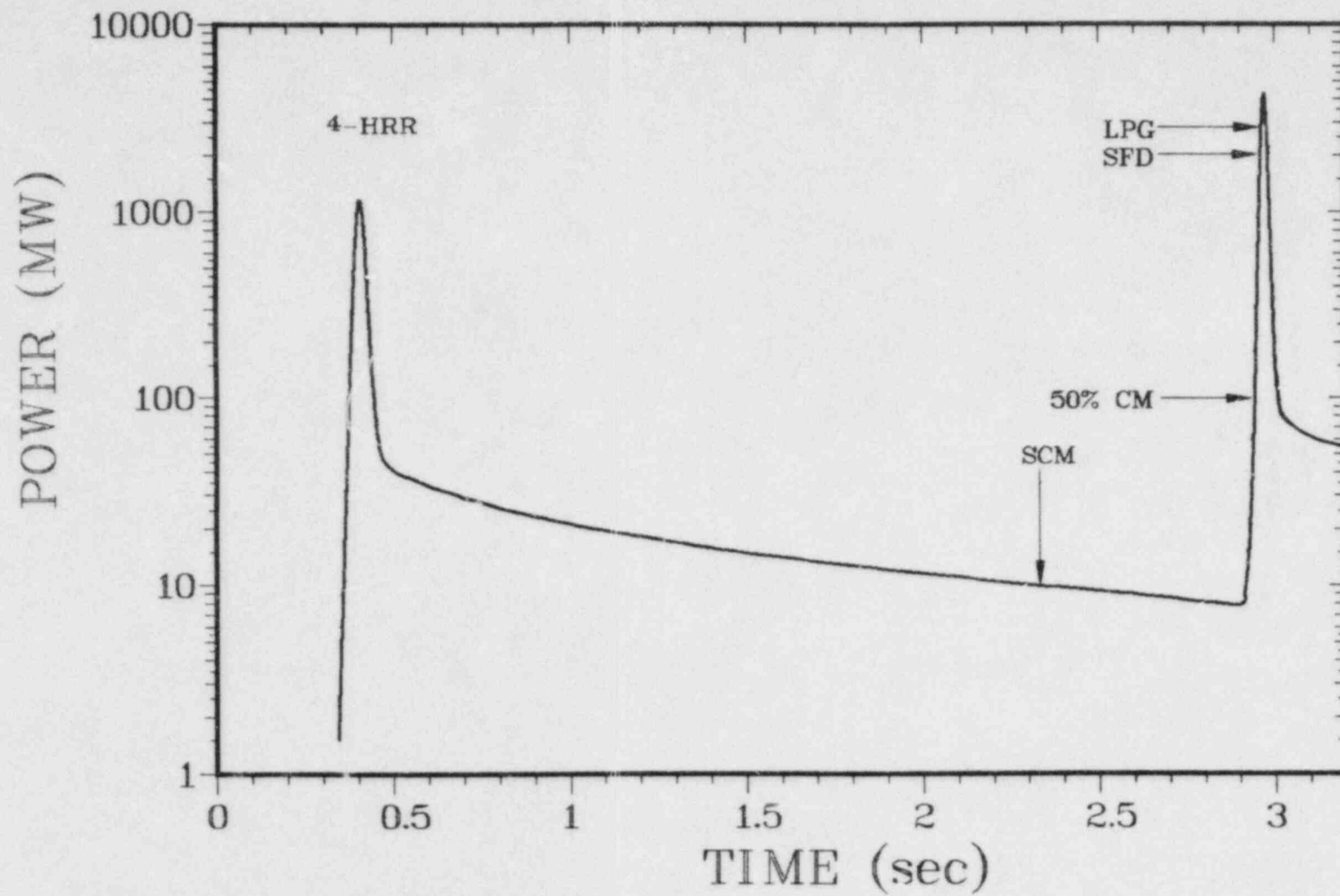Figure 2.1. Power Histories Used in the FD2/4 Series

4

Figure 2.2. Power History Used in the HRR Series

to preheat the fuel and melt the clad. The second pulse was delayed long enough to allow the temperature profiles to equilibrate and to allow most of the clad to relocate so that the fuel disruption could be observed directly.

The highly enriched fuel (40-67%) used in these experiments causes the energy deposition profile to peak near the surface. Fortu-nately, the ACRR reactor has a fast neutron spectrum, which helps minimize the peaking. In addition, gadolinium filters were used to further decrease the thermal and epithermal neutron flux. As a conse-quence, the peak to minimum energy deposition profiles were rather moderate (1.4 - 1.8). Furthermore, the reactor power transient pre-vented radial temperature inversions (in most experiments) by taking advantage of the radiative heat losses. The temperature profiles for experiments FD2.6, FD4.3, and HRR-2 are shown in Figures 2.3 a, b, and c.

A wide variety of disruption modes were observed in the experi-ments. Table 2.1 summarizes the heating conditions and the fuel properties of each experiment and gives a brief description of the disruption. This is a detailed table presented mainly as a basis of comparison between experiments and will not be discussed in detail in this report. However, a review of this table shows that the disrup-tion consisted of four major groups: (1) modest radial swelling in solid fuel (10-30%); (2) substantial swelling or frothing in molten fuel (4 to 6 times volume expansion); (3) solid state cracking or breakup of the fuel; (4) rapid liquid fuel dispersal. (Many experi-ments exhibit more than one form of disruption.) These different modes are illustrated with the three selected experiments mentioned earlier (FD2.6, FD4.3, and HRR-2).

In experiment FD2.6, the power levels and heating rates were relatively low (300-750 K/s), and fuel disruption consisted of signif-icant fuel swelling that began near the time of fuel melting in the interior of the fuel. The disruption is illustrated in Figure 2.4, which shows a few selected frames reproduced from the high speed films. Figure 2.3a shows the radial temperature profile through the fuel pin. As the fuel swelled it pushed out against the solid outer regions. Some of this solid fuel cracked and broke up, but it pro-vided little resistance to the swelling. The final volume of the swollen fuel mass was 6 to 7 times the original volume.

In experiment FD4.3, the power pulse occurred while the clad was melting; thus, fuel disruption and clad relocation occurred simultane-ously. The disruption consisted of solid fuel ejection through molten cladding. Approximately 10-20% of the fuel from a single fuel pellet was ejected from the unrestructured zone of the fuel pin. Figure 2.5 illustrates the observed disruption process in a few frames reproduced from the film. The temperature profiles are given in Figure 2.3b. At the time of fuel ejection (t=5.459 s) the unrestructured zone had an average temperature of 2140 K and was being heated at 2000 K/s. The ejection velocity of the fuel was initially 10 m/s, but slowed to 2 m/s after a few milliseconds. The ejection only lasted for 10 ms and

6
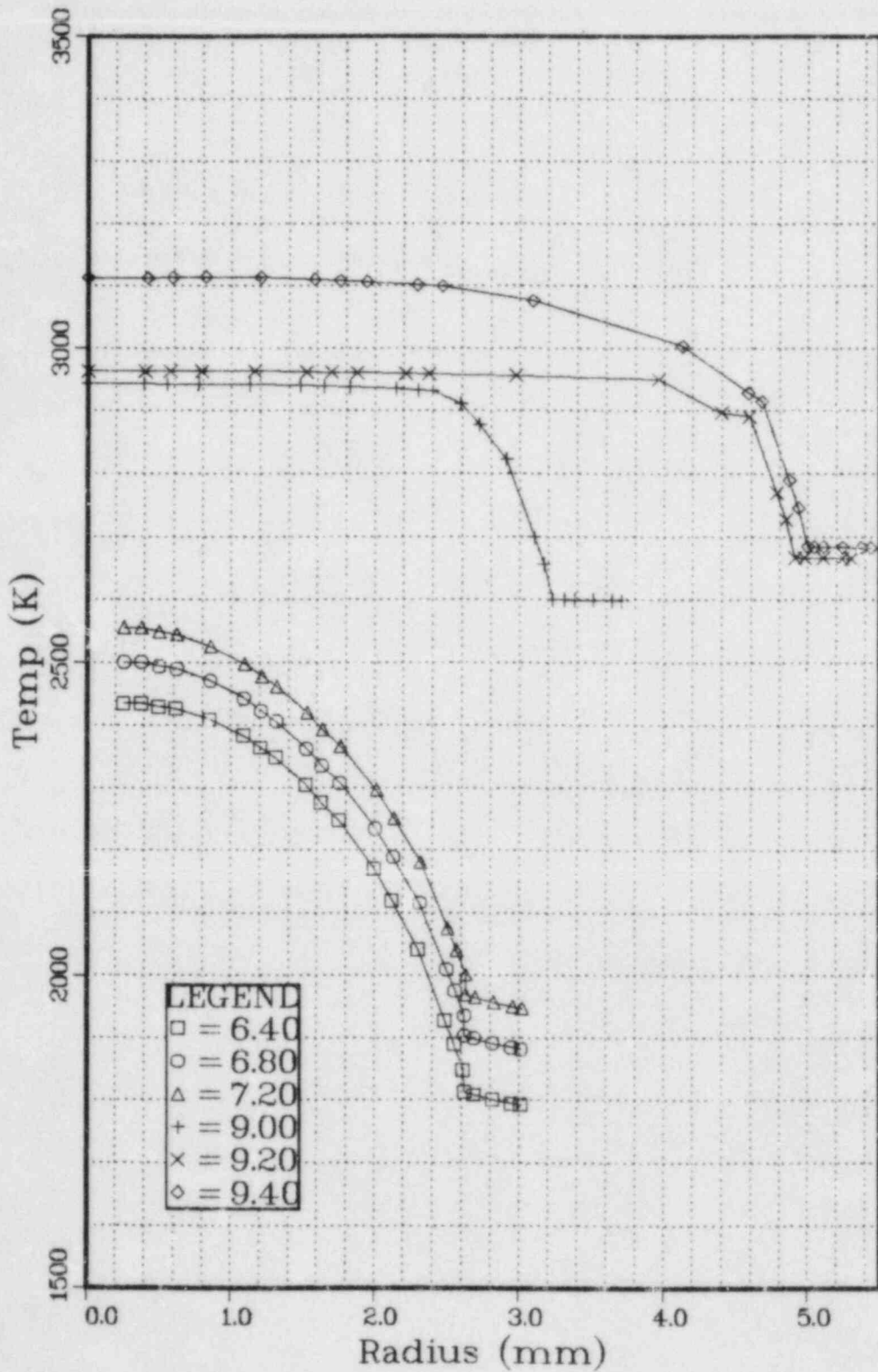
Figure 2.3a.   Radial Temperature Profiles for FD2.6
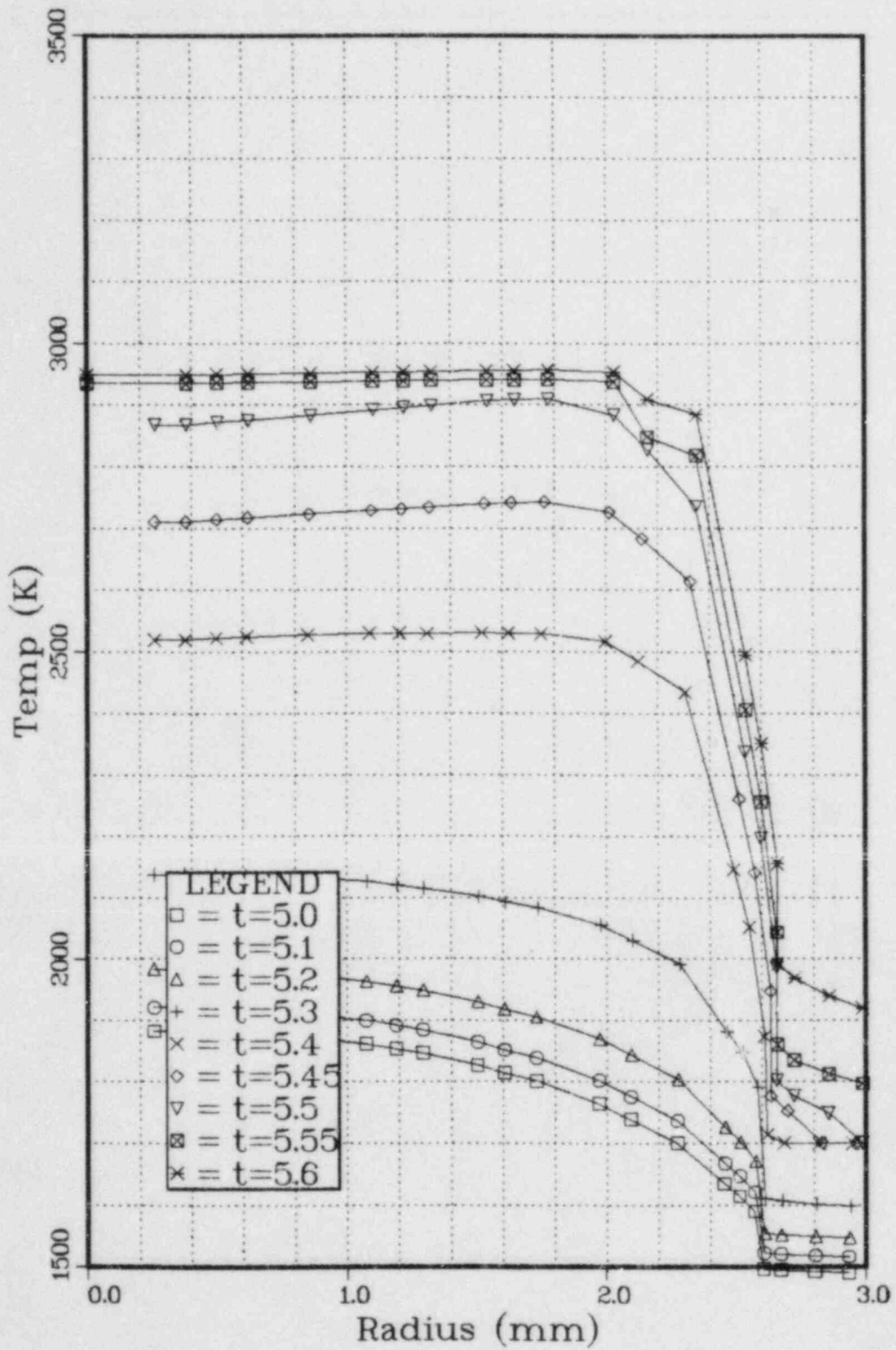
Figure 2.3b. Radial Temperature Profiles for FD4.3

8
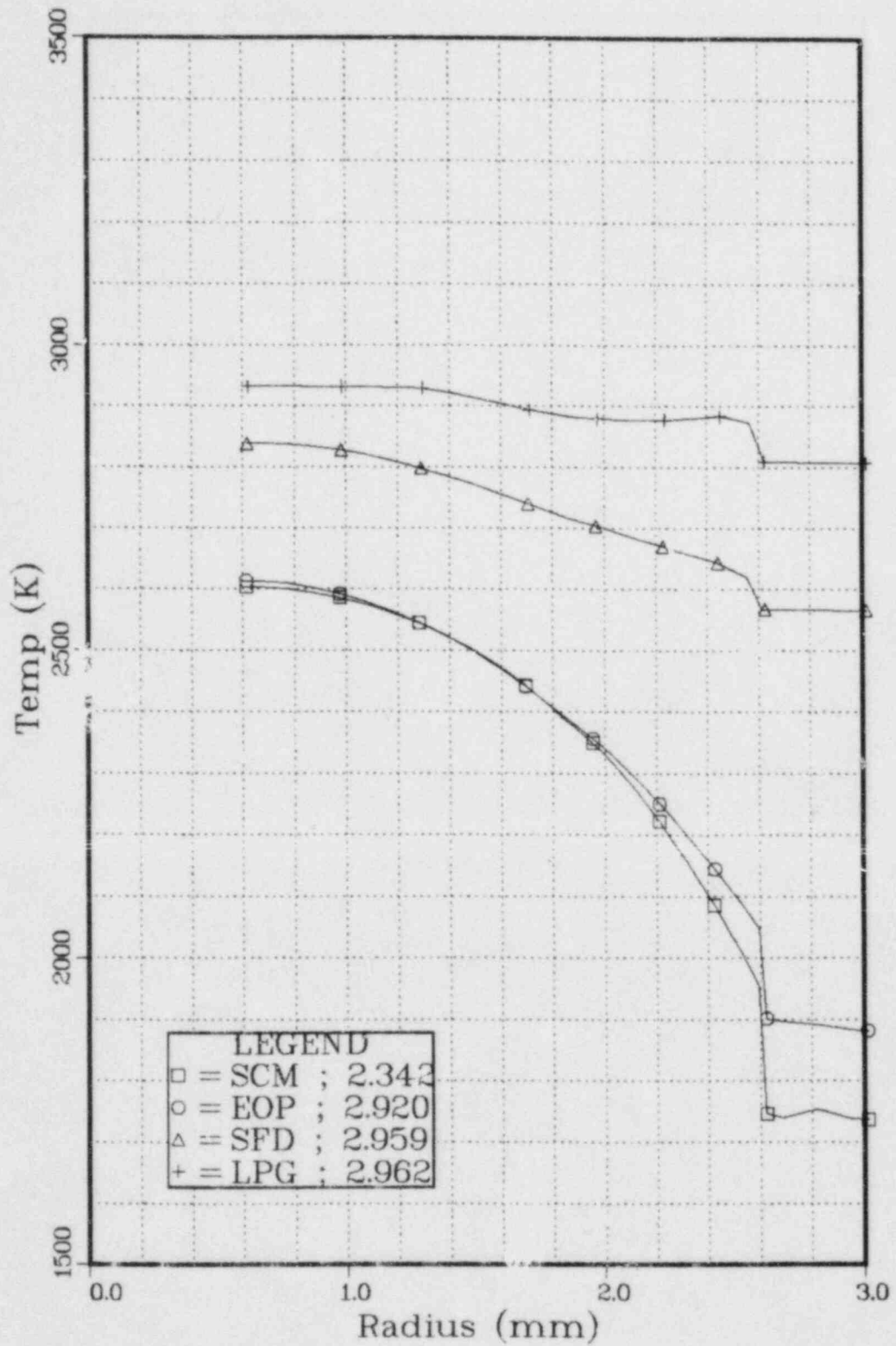
Figure 2.3c. Radial Temperature Profiles for HRR-2

TABLE 2.1

Summary of Heating Conditions and Disruption for Each FD Experiment

Experiment	Fuel Characteristic		Power History	Clad On/Off at Disruption	Power at Disruption	Disruption Model
FD	BU (a/o)	LHR (W/cm)			x Po	
2.4	5.3	283	-	On	6-8	Cracking and Breakup of Solid Fuel
2.6	5.3	283	1	Off	5-6	Massive Liquid State Frothing
2.7	8.3	151	1	On	4-5	Mild Solid State Swelling and Mild Breakup followed by Massive Liquid State Swelling
2.8	8.3	151	2	On	12-15	Mild Solid State Swelling and Sputtering Followed by Solid State Breakup and Liquid Frothing
4.0/2.5	Fresh Fuel		3	Off	12-14	Non-dispersive Ejection of Molten Fuel
4.1	4.2	329	3	Off	12-14	Rapid radial foaming beginning at fuel melting.
4.2	4.7	362	3	Off	12-14	Same as 4.1
4.3	5.5	251	2	On	14-17	Dispersive Solid State Break-up and Fuel Ejection Followed by Solid and Liquid State Swelling with Mild Sputtering
4.4	5.5	251	2	On	14-17	Same as 4.3 with No Fuel Melting - Used for PIE
4.5	4.5	430	2	On	14-17	Similar to 2.8 but German Fuel
HRR-2	4.7	333	4	50% On	250-300	Rapid Radial Spray of Near Molten Fuel
HRR-3	4.6	333	4	Off	200-250	Rapid Radial Spray of Molten Fuel
HRR-5	4.8	159	4	Off	180-200	Same as HRR-3
HRR-6	Fresh Fuel		4	Off	300-350	Same as HRR-3 with less energetic Dispersal

was followed by a quiescent period. After 30 ms of inactivity, the disruptive processes began again but with less vigor. This second disruptive phase consisted of mild sputtering and some swelling of solid fuel. Later, when the fuel began to melt (t=5.55s), significant fission product release was observed, along with rapid radial swelling or frothing. (The fission-product release was seen as a dark aerosol.)

In experiment HRR-2, fuel disruption occurred near the onset of melting ($T_{solidus}$), and the clad relocation was partially complete, with 50% of the clad still remaining on the fuel. The heating rate was very large (75,000 K/s). The disruption appeared as a rapid spray of apparent molten particles moving at 4 to 5 m/s. Six milliseconds later the SANDPIN calculations indicate that fuel vapor pressure further dispersed the fuel. Figure 2.6 illustrates the disruption process and Figure 2.3c shows the calculated temperature profiles for this experiment.

Table 2.2 illustrates the spectrum of disruption modes. It shows that the dispersive character (energy of the disruption) depends mainly on the heating rate but that other parameters, such as gas content, temperature, and temperature gradient, are also important. At the lower end of the dispersive spectrum is solid state swelling. In our experiment this type of behavior generally occurs at low heating rates (up to several hundred K/s), high temperatures (close to melting), or in fuel with very high gas content. The swelling is generally limited to 10 to 30% volume increases. Fission gas analyses indicate that this swelling is driven by vacancy diffusion and plastic creep of the fuel matrix.

Slightly more dispersive swelling occurs when the fuel begins to melt. In this case the volume increases in unconstrained geometries may be extremely large (6 to 7 times). This type swelling also occurs at moderate heating rates (up to several thousand K/s), and it occurs very rapidly (in a few tens of milliseconds). It might be more appropriate to call this type of disruption frothing or foaming since the volume increases are so large. Fission gas modeling shows that this swelling can be explained by non-equilibrium fission gas bubbles (bubbles with internal gas pressures greater than required for hydrostatic equilibrium) expanding to their equilibrium size when the fuel melts. This frothing or foaming process is dominated mainly by the large bubbles that occur on the grain boundary.

Solid state cracking is even more dispersive. This type of disruption was observed in several forms including non-energetic breakup of the fuel into large chunks, sputtering of small fragments, and energetic dispersal of significant quantities of fuel at large velocities (~10 m/s). This type of disruption was observed only when the fuel was heated at 6 to 16 x P_o (700 to 4,000 K/s) and also when the cladding was molten but still on the fuel. These conditions cause large temperature gradients in the fuel which, according to SANDPIN fission gas models, cause cracking by flooding the grain boundary with over-pressurized (non-equilibrium) fission gas bubbles.
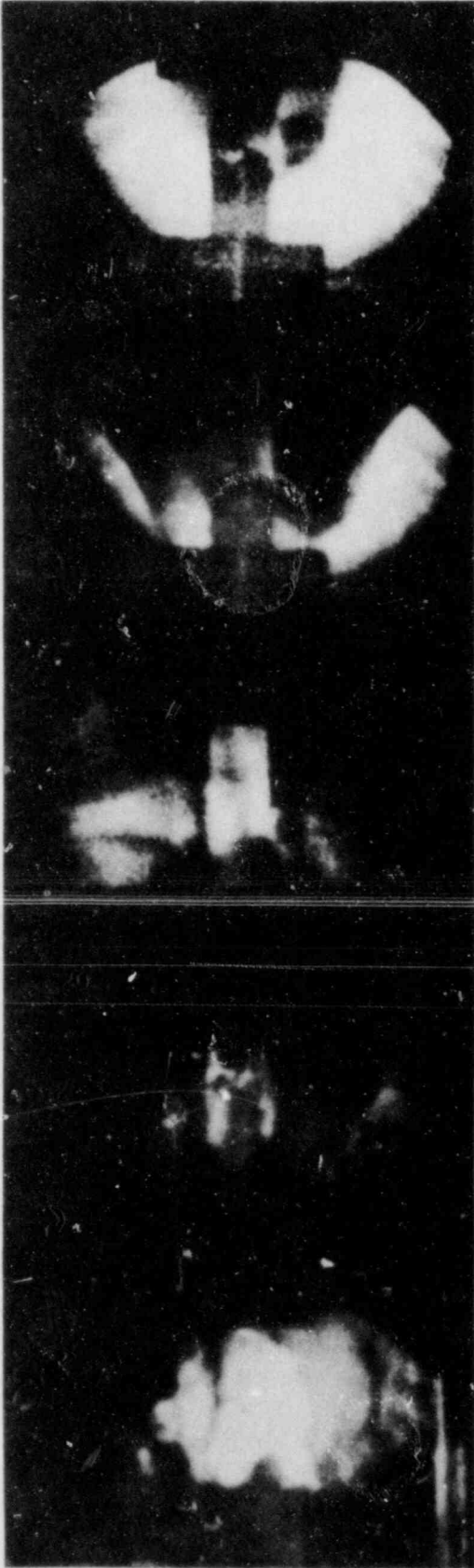
a) Aerosol Release from a
   Crack in the Cladding
   (t = 7.056 s)

b) Aerosol Coalescence and
   Clad Relocation
   (t = 7.395 s)

c) Start of Fission Gas
   Release (t = 8.451 s)

d) Start of Frothing with
   Fuel Surface Breakup
   (t = 9.158 s)

e) Final State of Fuel
   Frothing (t = 10.049 s)

Figure 2.4.   Selected Frames from Experiment FD2.6

a) Ejection of Solid Fuel
through Molten Cladding
(v=10 m/s; t=5.450 s)

b) Continued Ejection of
Solid Fuel (v=2 m/s;
t=5.463 s)

c) Quiescent Period
(t=5.482 s)

d) Mild Sputtering of Solid
Fuel(t=5.501 s)

e) Start of Fuel Swelling
(t=5.556 s)

Figure 2.5.   Selected Frames from Experiment FD4.3

13

(A)   50% Clad Melt Off
       (t = 2.950 s)
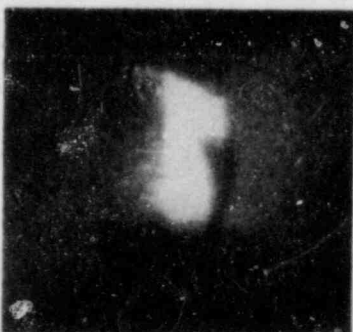
(B)   Fuel Sputtering
       (t = 2.956 s)
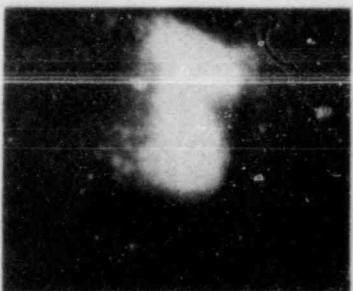
(C)   Start of Fuel
       Disruption
       (t = 2.959)
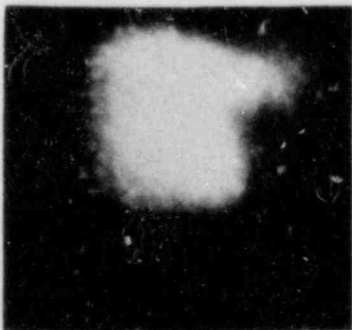
(D)   Loss of Pin Geometry
       (t = 2.962 s)

Figure 2.6. Selected Frames from Experiment HRR-2

14

TABLE 2.2

Spectrum of Disruption Modes

DISPERSIVE POTENTIAL	Non-Dispersive ⟶ Very Dispersive				
DISRUPTION MODES	Swelling/Frothing		Solid State Cracking		Liquid Dispersal
	Solid	Liquid	Breakup	Sputtering	Dispersion
HEATING RATE $T; \nabla T; C_{GAS}$	10 K/s	100 K/s	1,000 K/s		10,000 K/s
EXPERIMENTS	FGR, DEH		FD2/4		HRR, CABRI

Finally, very dispersive disruption is observed to occur when the fuel is heated at high heating rates (> 10,000 K/s), such as in the HRR or the CABRI[9] experiments. (In the HRR experiments the clad was molten and drained from the fuel pin at the time of disruption; however, in the CABRI experiments the disruption may occur while the clad is solid, molten, or molten and relocated, depending on the experiment.) This type of dispersive disruption is very similar to the frothing process except that it occurs much faster. The dispersion is driven by expanding fission gas bubbles at such large rates that they have enough energy to drive the fuel apart.

Heating rate or specific power is not the only parameter that governs the type of disruption. Clearly, other parameters such as fuel temperature, temperature gradient, and gas content are also very important. Also, because of large temperature differences in the fuel, one region of the fuel can be disrupted by one mode while another region disrupts by a different mode. For example, the center region may be molten and frothing while the outer cooler regions are cracking or sputtering. Thus the actual disruption that occurs is frequently a combination of modes.

These different types of fuel disruption can affect the ultimate outcome of an LOF accident. For example, if the first subassemblies to fail during an accident fail by energetic dispersal of solid fuel while the subassembly is voided, it is possible for the fuel to be swept out of the reactor by the streaming sodium vapor, possibly shutting down the excursion. On the other hand, if disruption occurs by swelling or frothing, the swollen fuel will fill the subassembly channels, thus inhibiting sweep out. Under these conditions other fuel and clad relocation processes must be postulated before neutronic termination can occur. This delay in the termination of the accident will increase the amounts of thermal energy deposited in the reactor core and, thus, increase the threat to the reactor containment.

3.0 FUEL DISRUPTION MECHANISMS

Fission gas, because of its early pressurization, is the primary disruption mechanism during the initial stages of reactor accidents. The SANDPIN code models the thermal, mechanical, and fission gas behavior in a fuel pin to predict the time and mode of disruption. The code and its results are described in more detail in another paper[10], but a brief overview of the fission gas model is presented here. The fission gas model is used to show how the disruption depends on various fission gas parameters as well as upon the heating conditions. This analysis describes a set of conditions, or criteria, that are required to produce the disruption. The disruption criteria are then graphically illustrated by means of a map which plots the criteria as a function of heating rate and fuel temperature.

3.1 REVIEW OF THE FISSION GAS MODEL IN SANDPIN

The SANDPIN code synthesizes the models of Matthews and Wood (NEFIG)[11], Ostensen (FISGAS)[12], and Worledge (TIGRS)[13], to calculate the fission gas behavior during transient heating conditions.* The purpose of the code is to predict the macroscopic fuel behavior by tracking the behavior of intra- and intergranular fission gas. Because of uncertainties in many of the microscopic properties governing diffusion and bubble migration, the code attempts to model the fission gas behavior in a simple way, yet still treat all of the important mechanisms. Consequently, all bubbles are assumed to be spherical, their average bubble size is used, and only Xenon fission gas is treated. In addition, the bubbles are not in equilibrium with the hydrostatic pressure of the fuel matrix.

Figure 3.1 illustrates the fission gas model. The intragranular fission gas field consists of uniformly distributed bubbles and dissolved fission gas. The intragranular bubble radii are quite small (on the order of 2 to 7 ηm). The bubbles coalesce and migrate to the grain boundary by biased and random diffusion. (Biased bubble migration occurs via temperature gradients. Stress gradient migration is not modeled in the code.) The dissolved gas migrates to the intragranular bubbles by random gas atom diffusion and by bubble sweep up. The code predicts that during a heating transient most of the dissolved gas collects in the intragranular bubbles and that these bubbles grow in size due to coalescence, vacancy diffusion, and dislocation creep processes. In addition, they collect on the grain boundary.

The grain boundary consists of large bubbles (radii = 1 to 3 μm), open porosity, and small bubbles ($r \sim 10\eta m$). The small bubbles have

DISSOLVED FISSION GAS

INTRAGRANULAR BUBBLES
(2-10 ηm)

$\frac{dT}{dR}$

LARGE
INTERGRANULAR
BUBBLES
(1μm)

SMALL
INTERGRANULAR
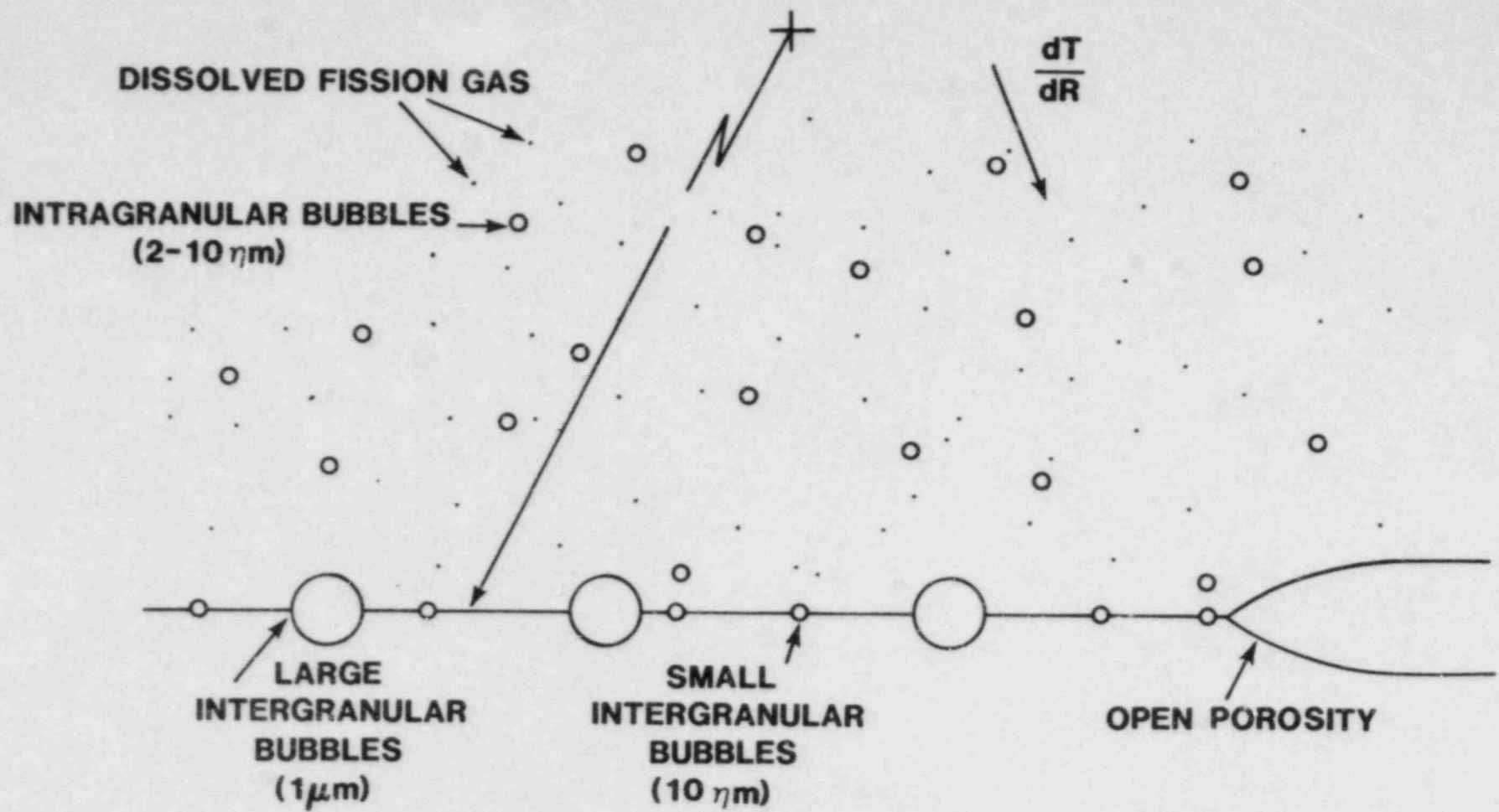BUBBLES
(10 ηm)

OPEN POROSITY

Figure 3.1. Intra- and Intergranular Fission Gas Model

migrated from the interior of the grain to the grain boundary. The intergranular bubble fields are allowed to coalesce among themselves and with the open porosity due to random and biased surface migration. In addition, these bubbles are allowed to grow in size via the vacancy diffusion and creep processes. All gas that coalesces with the open porosity is assumed to be released from the fuel pin.

Both the intra- and intergranular fission gas behavior is calculated at different radial locations in the fuel pin. Typically, the fuel pin is broken into columnar, equiaxed, and unrestructured zones. Each of these zones is further divided into a number of subzones to account for porosity differences.

The initial conditions for the fission gas parameters are taken from LANGZEIT[14] and from PIE studies. PIE measurements generally provide information such as grain size, porosity, bubble size, and total gas content. LANGZEIT provides details such as radial distribution of fission gas, fraction of dissolved fission gas, and fraction of intra- versus intergranular fission gas. These parameters are then combined with a consistent set of equations to determine other parameters such as initial bubble densities and pressures.

3.2 CONDITIONS FOR FUEL DISRUPTION

Three types of fuel disruption will be described: (1) solid state swelling, (2) liquid state frothing, and (3) solid state cracking. Liquid state dispersal is ignored since it is an extension of liquid state frothing. The approach used to describe these disruption modes is divided into two parts. In the first part, a condition or criteria (related to fission gas parameters) is specified that determines the mode of disruption and when it occurs. In the second part, the condition is used to determine a functional relationship between the fuel temperature and the heating rate by evaluating a simplified set of differential equations governing fission gas behavior.

3.2.1 Solid State Swelling

In the high speed films, volumetric swelling of 10% is easily detected. In addition, swelling significantly less than 10% will probably have limited impact on the accident progression. Therefore, significant solid state swelling will be said to occur when the fuel volume is increased by 10%. In terms of a single grain the fission gas swelling can be expressed as the increase in bubble volume divided by the grain volume. Therefore, the criteria for solid state swelling is

$$\frac{N_b T_o \int^{T_f} dV_b}{\frac{4}{3} \pi a^3} > f_{swell} \tag{3.1}$$

19

where

N_b = average number of bubbles per grain

V_b = average bubble volume

a = grain radius

f_{swell} = 0.1 => 10% volumetric swelling

The bubble volume and number of bubbles will change during the heating transient by coalescence, by migration to open porosity, by vacancy diffusion, and by dislocation creep processes. To evaluate equation 3.1 simply, several assumptions are made. It is assumed that the swelling is caused by the large grain boundary bubbles (because they have the weakest surface tension forces), that the number of bubbles (N_b) is known at T_o, and that this value remains constant during the heating transient. Thus, coalescence and loss mechanisms are neglected.

While the fuel is solid the bubbles can grow by vacancy diffusion and by dislocation creep. Only the vacancy diffusion is illustrated. Hull and Rimmer[15] showed that vacancies can diffuse up pressure gradients in the fuel lattice to the bubble. For grain boundary bubbles it is expressed as

$$\frac{dV}{dt} = \frac{4\pi \ wD_{gb} \ P_x \ \Omega}{kTH} \qquad (3.2)$$

where

wD_{gb} is the diffusion coefficient for vacancies on the grain boundary

wD_{gb} = $A \ e^{-\alpha/T}$

         $A = 6.9 \times 10^{-16}$

         $\alpha = 2.9 \times 10^4$

P_x is the excess pressure beyond equilibrium

$$P_x = \frac{nkT}{\frac{4}{3}\pi r_b^3} - \frac{2W_s}{r_b} \qquad (3.3)$$

20

Ω is the atomic volume of an uranium atom
$4.1 \times 10^{-29} \, m^3$

W_s is the modified surface energy $(2\gamma_s - \gamma_{gb})$

and   H   is a term that depends on the grain boundary coverage
fraction (for a coverage fraction of 0.1, H = 0.06)

Since dV/dt is equal to dV/dT x dT/dt, one can substitute equation 3.2 into equation 3.1 and solve for dT/dt if one assumes all fission gas parameters (r_b, P_x, etc) are constant. This yields a functional relationship between heating rate and fuel temperature which determines the threshold for 10% volumetric swelling. This relationship is expressed in the following equation.

$$\frac{dT}{dt} = \frac{N_b \; 3\pi \; r_b \; \Omega \; A \; P_x}{f_{swell} \; k \; H} \left[T \, e^{-\alpha/T} - T_o \, e^{-\alpha/T_o} \right] \qquad (3.4)$$

The asymptotic solution to exponential integrals for large arguments was used to obtain this expression.

This equation shows how the swelling depends on the fission gas parameters. Because this equation is proportional to N_b, r_b, and P_x, it is strongly dependent on the gas content, with increasing gas content causing increased swelling. In addition, the linear dependence on r_b means that the larger bubbles dominate the swelling process. Since the grain boundary bubbles (though few in number) are generally the largest, they are the ones that dominate swelling.

Figure 3.2 presents a map of fuel disruption, with boundaries marking the fuel temperature and the heating rate at which different types of disruption will occur. This approach graphically illustrates the conditions governing fuel disruption. The threshold for vacancy diffusion-induced volumetric swelling is plotted as a function of heating rate and fuel temperature in Figure 3.2 (solid line). The other disruption modes shown on this figure will be described later. The curve for vacancy diffusion-induced swelling assumes an initial fuel temperature of 2000 K. The fission gas parameters used to calculate this curve are given in Table 3.1 for a fuel pin with 5.3 a/o burnup.

The curve in Figure 3.2 shows that for significant swelling to occur by vacancy diffusion, the heating rate must be <100K/s. The temperature dependence of this threshold is governed by the exponential nature of the grain boundary vacancy diffusion coefficient. This curve should not be taken too literally. It is only meant to illustrate the nature of the swelling. In addition, the location of this boundary on the disruption map will move around, depending on the fission gas parameters such as gas content, bubble size, and number of bubbles.
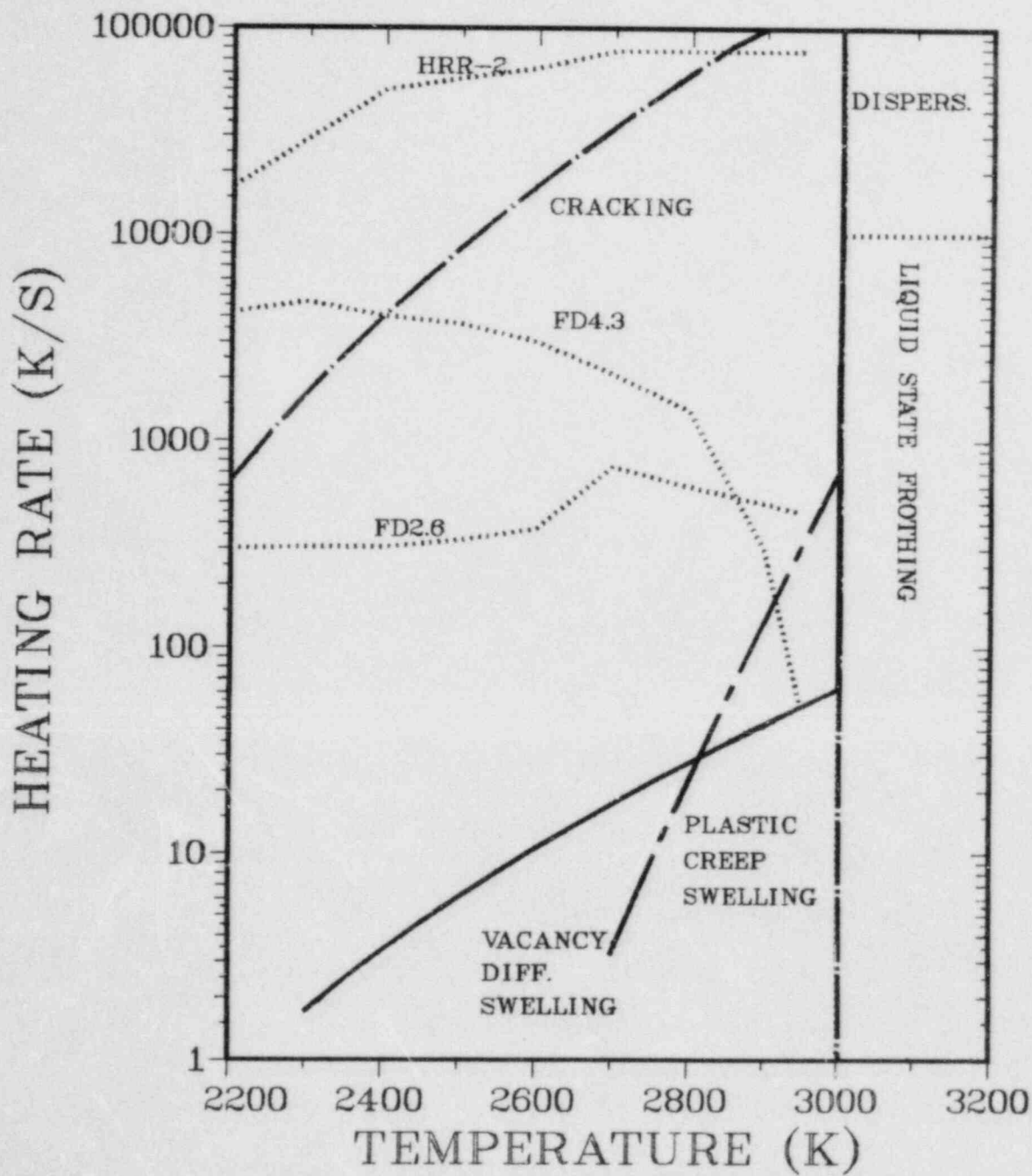
Figure 3.2. Fuel Disruption Map

TABLE 3.1

Intergranular Fission Gas Parameters for 10% Solid State Swelling and Liquid Frothing

---

N_b = 8 large grain boundary bubbles per grain

r_b = 1 x 10^{-6} (m)

n = 4 x 10^9 atoms per bubble

W_s = 0.5 J/m^2

a = 5 μm

k = 1.38 x 10^{-23} J/molecule-K

P_h = 2 x 10^5 N/m^2

Another mechanism that can contribute to solid state swelling is plastic creep (power law creep) of the fuel matrix. The approach used to calculate the swelling condition for this mechanism is identical to one used for vacancy diffusion and is not repeated in this report. Equations governing the rate of bubble volume increase by plastic creep are found in References 13 and 16.

The threshold for swelling caused by plastic creep is plotted as a dotted line in Figure 3.2. It dominates vacancy diffusion swelling at high temperatures and at high heating rates. This is due to the stronger exponential dependence of the power law creep rate, which is equivalent to the diffusion coefficient for vacancy diffusion. (The power law creep rate given by Slagle[16] is used, rather than those suggested by Worledge.[13]) Swelling is predicted to occur near the fuel melting temperature (within 200 K); however, the heating rates may be up 300 K/s.

To illustrate how the fuel disruption map works for swelling, an example is used in which fuel is heated at a heating rate of about 100 to 300 K/s. This is roughly equivalent to a fuel pin operating at nominal power in a voided subassembly. Then, when the fuel temperature reaches approximately 2800 K, the disruption map predicts that the fuel will have swollen by at least 10%. As the fuel continues heating it will continue swelling until fuel melting begins (around 3000 K). The swelling is limited to a relatively narrow range of 10 to 30 volume percent at the onset of fuel melting. When the melt temperature is reached another model must be used to predict the behavior.

3.2.2 Fuel Disruption by Liquid Frothing

At moderate heating rates (500 to 4000 K/s) fuel disruption consists of a very large volume increase at the onset of melting. SANDPIN treats this disruption very simply by allowing the non-equilibrium bubbles (whose density, pressure, and radius are known from the solid state fission gas calculations) to instantaneously grow to their equilibrium size. Thus, the condition for liquid frothing is that the fuel temperature exceeds the solidus temperature.

$$T > T_{solidus} \tag{3.5}$$

In reality, the bubble equilibration is a gradual process and takes place while the fuel is passing through the heat of fusion. For the development of the disruption map, melting is assumed to occur at 3000 K even though irradiated, mixed oxide fuel has a solidus temperature near 2930 K, and fresh UO_2 has a melting point near 3130 K. Thus, the disruption map has a vertical line at 3000 K to mark the onset of fuel melting.

The potential for volume increase is evaluated in the same manner as solid state swelling. The increase in volume is therefore equal to the number of bubbles per grain times the equilibrium volume of the bubbles divided by the initial grain volume.

$$W_{froth} = \frac{N_b \, V_e}{\frac{4}{3} \pi a^3} \tag{3.6}$$

where V_e is the equilibrium volume of the bubble. It can be calculated by iteratively solving the following equation to balance the surface tension forces with the hydrostatic pressure. An ideal gas is assumed.

$$V_e = n \, kT \left[P_h + \frac{2W_s}{\left[\frac{3V_e}{4\pi} \right]^{1/3}} \right]^{-1} \tag{3.7}$$

where

n = the number of atoms in a bubble

k = the Boltzman constant

$W_s = 2\gamma_s - \gamma_{gb}$, the modified surface energy

24

To evaluate these expressions, the average number of bubbles per grain boundary N_b, the number of atoms per bubble (n), and the hydrostatic pressure (P_h) at the melt temperature must be known. These quantities are given in Table 3.1. For a hydrostatic pressure of two atmospheres, these constants yield a frothing potential of 6.0 (i.e., the unrestructure fuel has the potential to increase its volume by a factor of six). Since most of the fission gas is concentrated in the unrestructured portion of the fuel, the total potential for swelling is less, but this number demonstrates the tremendous potential for fuel frothing. Clearly, in a reactor there is no room for these types of volume increases; consequently, when melting and significant frothing occurs it will pressurize and attempt to force the molten fuel out of this region. Other potential driving pressure sources such as gravity, sodium vapor, and steel vapor will compete with viscous flow and the potential plugging processes to determine the overall fuel motion.

At very large heating rates the rapid bubble expansion can cause the fuel to disrupt as a fine spray of molten particles rather than froth. This transition from non-dispersive frothing to energetic dispersal is not evaluated in this paper. However, it has been experimentally observed to occur at heating rates near 10,000 K/s. Thus, the disruption map has a horizontal line at 10,000 K/s to mark the transition from frothing to dispersal.

3.2.3 Cracking and Breakup of Solid Fuel

The condition for cracking of solid fuel is based on the theory of brittle fracture by Cottrell[17] and was applied to fission gas-induced cracking of fuel by Worledge[13] and Dimelfi.[18] Cottrell's theory states that cracking occurs when the strain energy around a grain boundary defect has enough energy to separate the grain boundary by causing point defects to migrate to the grain boundary. For fission gas in fuel, a grain boundary bubble is assumed to be a defect with an incipient crack. The pressure in the non-equilibrium bubbles stresses the fuel matrix around the bubble in an amount proportional to the potential energy of pressurized gas in the bubble. If the PdV work of expanding the gas through the crack exceeds the energy required to create new surface area (by extending the crack such that it interlinks with the neighboring bubbles), then the fuel matrix will crack. Figure 3.3 illustrates the cracking process and the fracture analysis yields the following equation.

$$P_{crack} > \frac{2W_s}{\delta} \left[1 + \frac{\pi \left(R_{eff}^2 - r_b^2 \right) \delta}{V_b} \right] \tag{3.8}$$
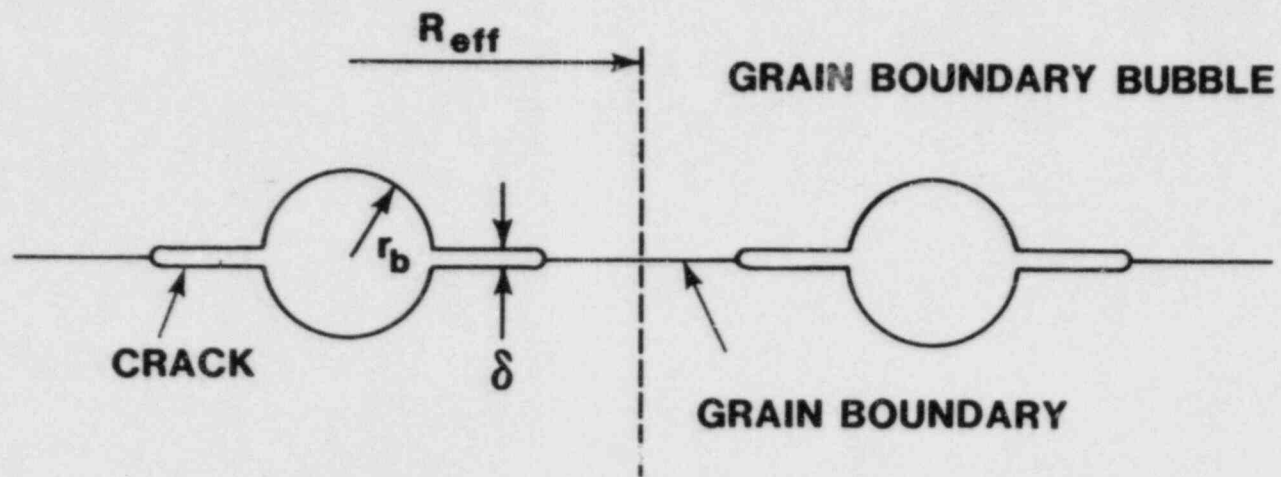
Figure 3.3. Grain Boundary Cracking Model

where

P_{crack} is the pressure in the grain boundary bubble required to crack the matrix

R_b is the average radius of the bubble

R_{eff} is the mean cell radius between grain boundary bubbles

δ is the crack height, $\delta = 2\eta m$

For very large bubbles this equation reduces to

$$P_{crack} > \frac{2W_s}{\delta} \tag{3.9}$$

which is the same criteria developed by Worledge. However, the SANDPIN calculations indicate that cracking is caused by the small intragranular bubbles. In this case the cracking criteria becomes

$$P_{crack} > \frac{2W_s N_o}{\delta N_{sb}} \tag{3.10}$$

where

$$N_o = \frac{2\pi a^2 \delta}{V_{sb}} \tag{3.11}$$

N_{sb} is the number of small bubbles per grain, V_{sb} is the volume of the small bubbles, and $R_{eff} \gg r_{sb}$ is assumed. SANDPIN predicts that the small grain boundary bubbles have a pressure that is always very near the large bubble cracking pressure, regardless of the heating rate and the temperature. Therefore, setting $P_{crack} = 2W_s/\delta$ produces the final approximation to the cracking criteria.

$$N_{sb} > N_o \quad \Longleftrightarrow \quad N_{sb} > \frac{2\pi a^2 \delta}{V_{sb}} \tag{3.12}$$

This equation states that the number of small grain boundary bubbles must exceed N_o to cause cracking. Typically, N_o is on the order of 7.5×10^4 bubbles per grain using the values for a and δ given earlier, and assuming a bubble radius of $10\eta m$. The small bubbles are much more effective in causing the cracking because there is a large source of them in the grain (typically 3×10^5). Thus, they can dramatically reduce the distance required to interlink the bubbles.

27

To evaluate this expression, the relationship between the number of small grain boundary bubbles and the heating conditions must be known. For sufficiently large temperature gradients the migration of intragranular bubbles to the grain boundary is dominated by biased diffusion. If all loss processes on the grain boundary are neglected (coalescence, migration to open porosity, bubble growth), then the number of bubbles on the grain boundary can be expressed as

$$\frac{dN_{sb}}{dt} = \frac{v \; N_{intra}}{a} \qquad (3.13)$$

where N_{intra} is the number of intragranular bubbles

v is the migration velocity of the intragranular bubbles

$$v = \frac{3 \; \lambda \; Q_s \; dT/dR \; D_b}{r \; kT^2}$$

D_b is the bubble diffusion coefficient

$$D_b = Be^{-\beta/T} \qquad \begin{matrix} B = 3.5 \\ \beta = 4.53 \times 10^4 \end{matrix}$$

Q_s 6.97×10^{-19} J/molecule, heat of transport

λ 0.34 ηm, surface diffusion boundary layer thickness

dT/dr is the local temperature gradient (K/m)

These equations can be solved to determine a functional relationship between heating rate and fuel temperature, resulting in the following equation when the initial number of bubbles on the grain boundary is taken to be zero.

$$\frac{dT}{dt}\bigg|_{crack} < \frac{N_{intra}}{a \; N_o} \; \frac{3 \; \lambda \; Q_s \; dT/dR \; B \; e^{-\beta/T}}{r \; k \; \beta} \qquad (3.14)$$

This equation is plotted as a chained-dot curve in Figure 3.2, given the fission gas parameters listed in Table 3.2. The parameters listed are taken from the unrestructure portion of a 5.3 a/o burnup fuel pin.

TABLE 3.2

Fission Gas Parameters for the Crack Criteria

N_o	7.5×10^4 small intergranular bubbles per grain
r_{sb}	10 ηm
N_{intra}	3.0×10^5 intragranular bubbles per grain
δ	2ηm
a	5 μm
dT/dR	2000 K/mm

Equation 3.14 clearly shows that the cracking criteria depends linearly on temperature gradient. If the temperature gradient is large, then moderate heat rates will satisfy the cracking criteria at temperatures below the melt temperature. During the power transient the temperature gradients are strongly dependent on whether clad is on or off the fuel. When the cladding has already relocated, the gradients are on the order of 100-500 K/mm, but when the clad is molten and still attached to the fuel the gradients may be as large as 2000 K/mm. This can make the difference between cracking or not cracking the fuel matrix. In Figure 3.2 no cracking is shown below heating rates of 1000 K/s. This was done to demonstrate that at low heating rates the temperature profiles are too flat to allow cracking.

At high heating rates ($>10^5$ K/s) the disruption map predicts fuel melting rather than cracking. This is because there is not enough time for the intragranular bubbles to diffuse to the grain boundary. Thus, the disruption mode degenerates to molten fuel disruption which, at these heating rates, exhibits itself as a dispersive spray.

The disruption map just presented graphically illustrates the disruption modes and how these modes depend on the heating conditions. The dependence on fission gas parameters is not explicitly shown in the map, but it was described in the development of the disruption criteria. To develop this map, the fission gas model used by SANDPIN was greatly over-simplified; thus, the map is only useful for demonstration purposes and should not be used for predictive analysis. In addition, the range of application for this map is limited because it is based only on four types of disruption behavior. Clearly, other modes of disruption may exist, especially for accident scenarios that cover different ranges of heating conditions and fuel types other than those investigated in the FD program. For example, during disruption in TOP accidents the cladding is still solid when fuel melting occurs.

This will probably cause a different type of disruption than mentioned
in this report. Also, low gas content fuel (low burnup) will probably
display different disruptive behavior.

3.3 APPLICATION OF THE DISRUPTION MAP AND RESULTS OF SANDPIN

Figure 3.4 reproduces the disruption map with the heating condi-
tions for the three example experiments (FD2.6, FD4.3, and HRR-2)
superimposed on the plot.

For experiment FD2.6, the heating rate initially started at 300
K/s and increased to 750 K/s during the power rise to 6 x Po. The map
shows that little solid state swelling should occur (<10%), but that
disruption should consist of liquid frothing or foaming beginning at
the fuel melt temperature. This was indeed observed. Because fuel
melting begins in the center and works its way to the surface, the
total swelling is not instantaneous but occurs gradually. As the
interior of the fuel pin swells it increases the pin radius, which
also increases the radiation heat losses. This effect is included in
the SANDPIN analysis. Figure 3.5 shows the calculated and measured
fuel pin radius as a function of time. The magnitude and the rate of
volume increase are accurately modeled by SANDPIN. (The total volume
increase was very large, seven times the original volume.) The calcu-
lations predict that the frothing begins earlier than observed (~200
ms), but this is probably due to the use of the solidus as the thres-
hold temperature for frothing rather than a temperature intermediate
between the liquidus and solidus.

In a similar experiment, FD4.1, the heating conditions were
nearly identical except that at near melting the heating rates were a
few thousand K/s (12 x P_o) rather than several hundred (6 x P_o). The
fuel behavior was nearly identical to that of FD2.6 (as indicated by
the disruption map) except that the foaming was much more rapid
because of the higher heating rate. This confirms an earlier hypoth-
esis that the energetics of the frothing process were dependent on the
heating rate (power level).

In experiment FD4.3, the clad was on the fuel up to the time of
fuel melting. The disruption map shows the heating conditions for
this experiment. It starts off with heating rates near 4000 K/s and
then, because of clad melting, the heating rate decreases as heat is
rapidly transferred to the clad, which has a large heat capacity and
good thermal contact with the fuel. The map shows that fuel disrup-
tion should first occur as solid state cracking while the fuel temper-
ature (unrestructured zone) is 2400 to 2500 K. Following this
cracking, heating continues, although at a slower rate, and some sig-
nificant solid state swelling prior to melting and liquid state
frothing is expected exactly as the films and thermal calculations
showed.

The cracking criteria used in SANDPIN compares the energy
required to interlink the fission gas bubble by cracking to the poten-
tial energy in the bubbles (equation 3.8). When this ratio exceeds
one, cracking is said to occur. Figure 3.6 illustrates the cracking
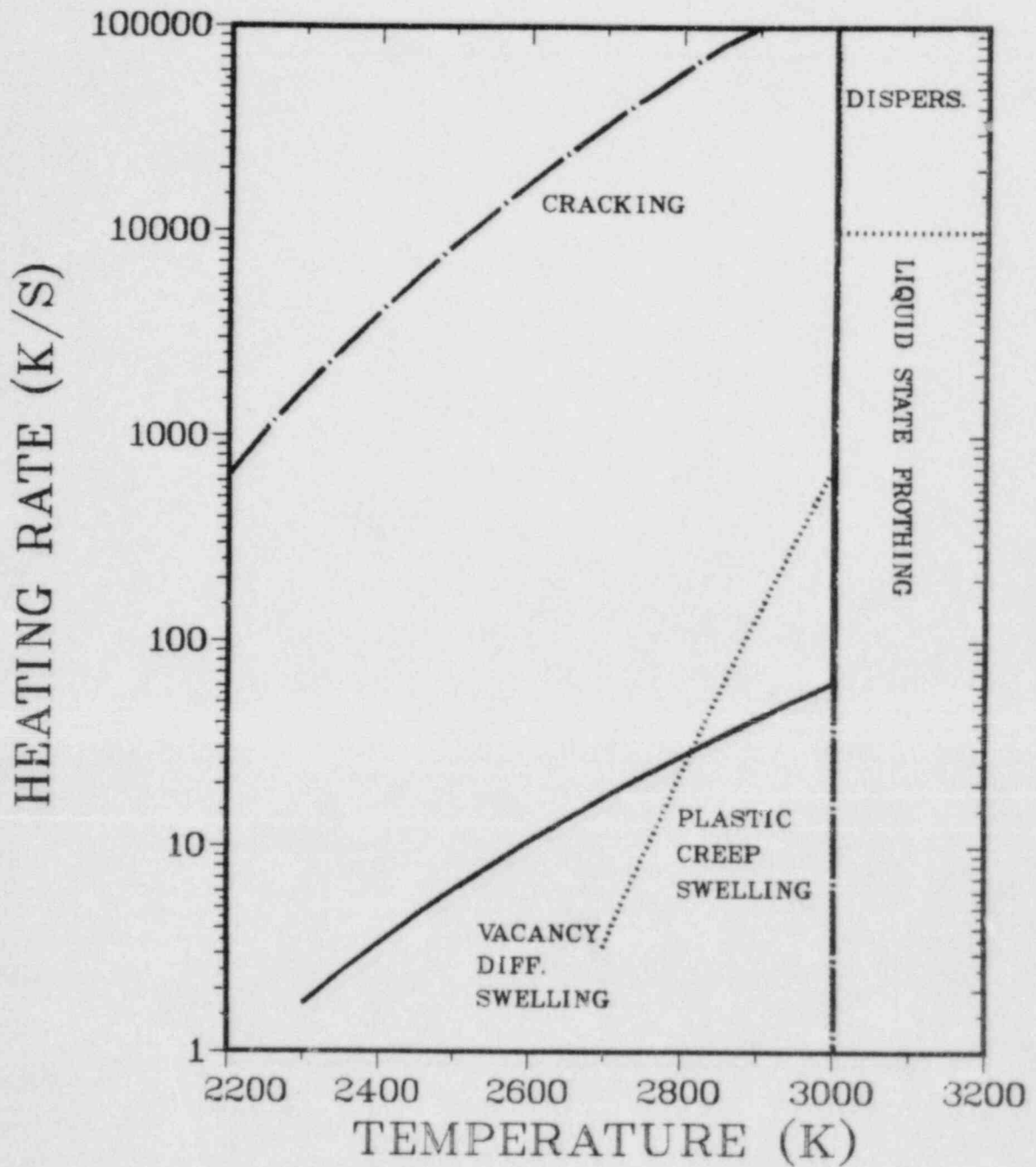
30

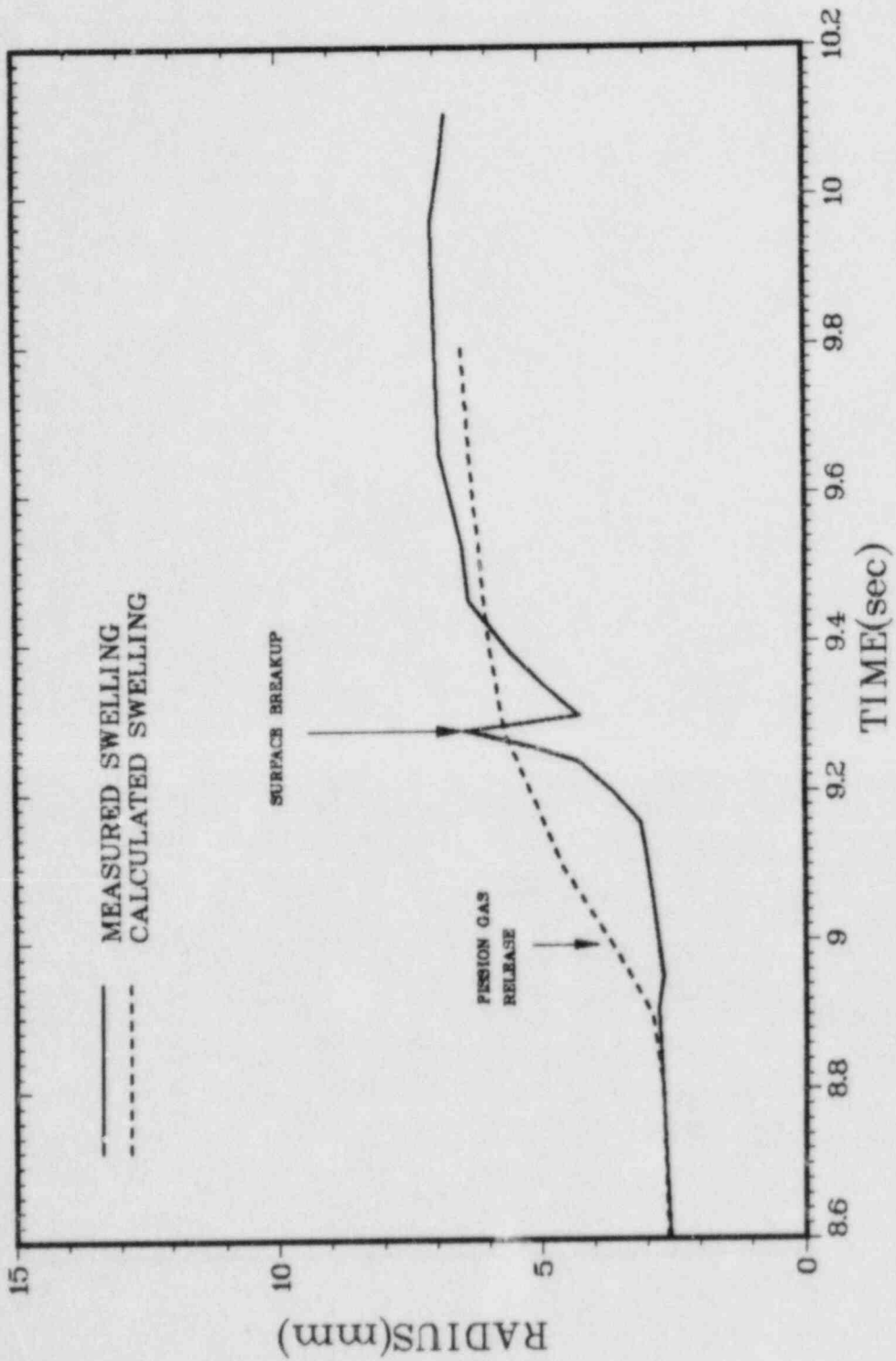Figure 3.4. Fuel Disruption Map for Experiments FD2.6, FD4.3, and HRR-2

31

Figure 3.5. Calculated and Observed Fuel Frothing in Experiment FD2.6
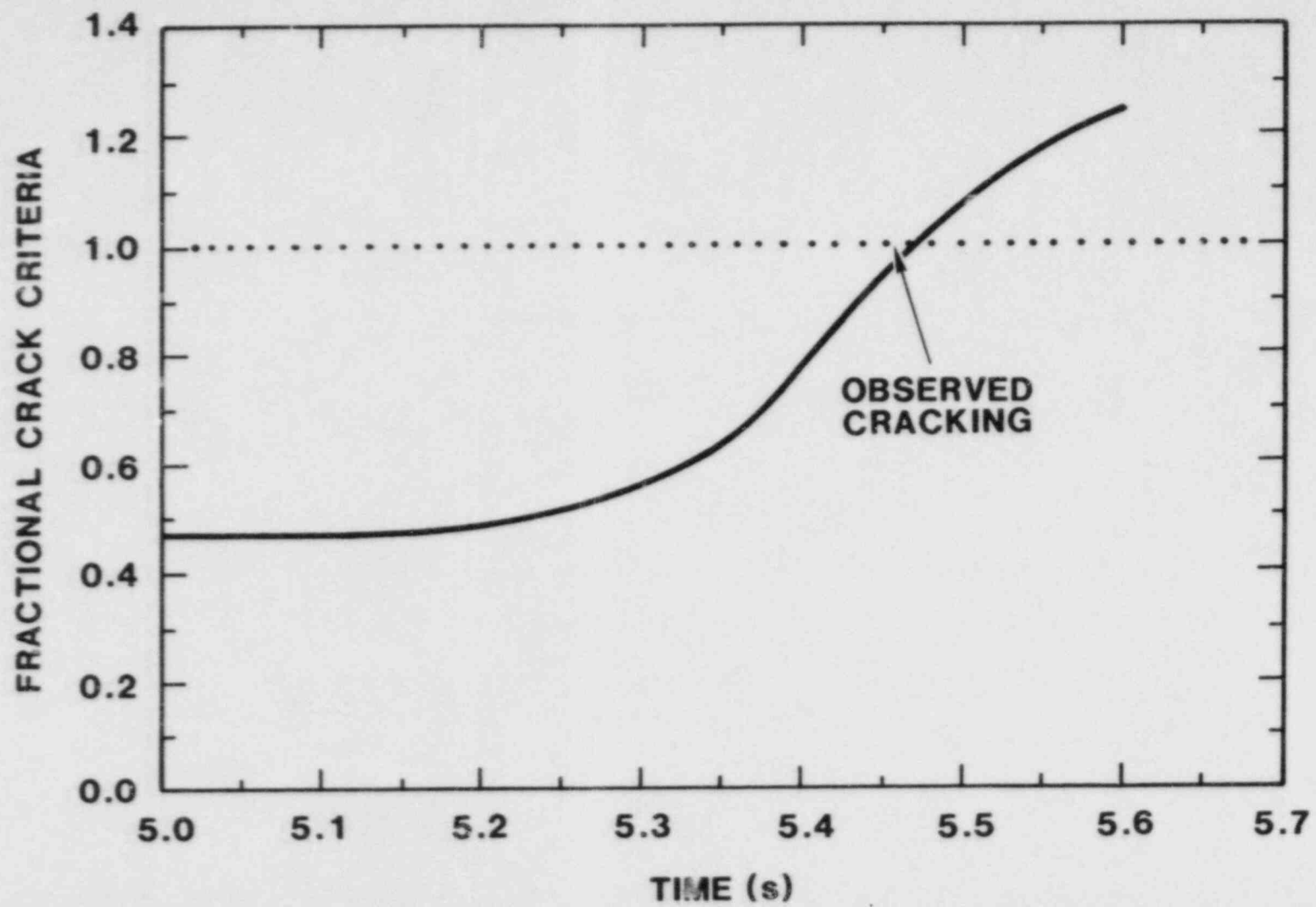
Figure 3.6. Calculated and Observed Cracking in Experiment FD4.3

criteria and compares it to the observed time of cracking. As shown, the calculations and observations are in very good agreement, reflecting the occurrence of a major phenomenon (flooding of the grain boundary with small bubbles) which is not strongly dependent on the detailed values and constants used in the fission gas calculation.

The heating conditions for the HRR-2 experiment are also shown in the Figure 3.4. The heating rates start near 17,000 K/s and increase to 70,000 K/s. Whether clad is on the fuel or off, fuel disruption is expected to occur at the onset of fuel melting or very near it. This was observed in all the HRR experiments. Because of the large heating rates ($\sim 10^5$ K/s), the disruption appeared as a energetic spray of molten or near molten particles, as shown in Figure 2.6.

In a few experiments (FD2.7 and FD2.8) significant solid state swelling was observed. The fuel for these experiments had a high fission gas content due to its high burnup 8.3 a/o and low linear heat rating. In both experiments swelling occurred while the clad was still on and exhibited itself as an axial or longitudinal crack in the molten or near-molten cladding. The maximum fuel temperature at the start of swelling was 2500 K and the final volume expansion was ~47%. These experiments are evidence for the sensitivity of the swelling to fission gas content, and show that higher gas content does not necessarily mean more dispersive disruption. In these experiments and at these heating rates, the higher gas content caused earlier, less energetic disruption.

4.0 CONCLUSIONS AND SUMMARY

This paper reviews the experiments and analysis performed for the FD program and summarizes some of the more important observations and results. The experiments provide a large data base for understanding the behavior of fuel during LMFBR accident heating conditions. The information gained from these experiments was used to develop a fuel pin code, SANDPIN, that models the thermodynamic and fission gas behavior to predict the time and mode of fuel disruption. A few selected experiments were described which illustrated the fission gas mechanisms causing fuel disruption.

The experiments show that fuel disruption consists of a spectrum of modes with dispersive characteristics that range from very mild to very energetic. The observed disruption modes consisted of modest radial swelling in solid fuel (10 to 30%), substantial frothing in molten fuel (4 to 6 times the original volume), solid state cracking, and very rapid liquid fuel dispersal. The dispersive character of these disruption modes depends mainly on heating rate, but other parameters, such as fission gas content and temperature gradient, play important roles in the disruption process.

A fuel disruption map was presented that plots heating rate as a function of fuel temperature to illustrate the different criteria for disruption. Although this approach to describing fuel disruption oversimplifies the fission gas processes modeled by SANDPIN, it does illustrate the criteria used to determine which fuel disruption mechanism is dominant and on what major fission gas parameters it depends.

The major fuel disruption modes and the dominant fission gas mechanisms causing the disruption are described below.

The least dispersive fuel disruption consisted of solid state swelling. The analysis and experiments showed that the swelling occurs at low heating rates (up to several hundred K/s) and at high fuel temperatures (T > 2600 K). The swelling is dominated by the growth of large intergranular fission gas bubbles by vacancy diffusion and by dislocation creep. The swelling is generally limited to volume increases of 10 to 30%, but it is strongly dependent on fission gas content. Higher fission gas content causes the swelling to occur at lower temperatures and at higher heating rates.

When fuel melting occurs, the disruption is slightly more energetic than in the previous case, and it consists of frothing or foaming of liquid fuel. This mode of disruption is dominant at moderate heating rates (500 to 4000 K/s), but always occurs in some degree when fuel melting begins. The frothing is caused by the very rapid equilibration of over-pressurized fission gas bubbles. Again, the large intergranular fission gas bubbles are most responsible for the large volume increases observed in this disruption mode. Typical volume increases may be as large as 6 to 7 times the original volume. At very large heating rates (>10,000 K/s) the frothing process makes a transition to a rapid dispersal of liquid fuel. This transition

occurs because the kinetic energy of the expanding bubbles (due to their pressure equilibration) is enough to drive the fuel apart.

Perhaps the most interesting mode of disruption was of solid fuel. This type of disruption consisted of breakup of large chunks, sputtering, and energetic dispersal of finely divided pieces of fuel. The experiments and analysis show that this mode of disruption requires large temperature gradients in the unrestructured fuel. This condition occurs at moderate heating rates ($\sim$4000 K/s, 6-16 x ?$_0$) when the clad is partially molten but still on the fuel (prior to clad relocation). The analysis indicates that cracking occurs because non-equilibrium grain boundary bubbles stress the fuel matrix, causing small cracks around the bubble. When the potential energy of the bubble pressure (proportional to stress energy) exceeds the energy required to crack the grain boundary surface area by interlinking all fission gas bubbles, then cracking is said to occur. This can occur not only by the increase of the bubble pressure, but also by the increase in the number of bubbles on the grain boundary (which reduces the stress energy per bubble required to crack the matrix). The cracking process is dominated by small intragranular fission gas bubbles that migrate to the grain boundary under the influence of large temperature gradients.

The high resolution data base provided by the FD experiments are extremely useful in the development of fuel disruption models. This has resulted in the joint development of the SANDPIN code that can predict the time and mode of fuel disruption. The code does an excellent job of predicting the disruption modes in all experiments. The code and experiments are therefore useful for verifying initiation phase fuel behavior models used in system analysis codes such as SAS.

5.0 FUTURE WORK

The initial mode of fuel disruption is important in determining the severity of LMFBR accident scenarios. However, it is just one aspect of the initiation phase accident behavior. Ultimately, the subsequent reactivity feedback of fuel and clad relocation must be known before the outcome of an accident scenario can be predicted. The study of fuel and clad relocation is the subject of the follow-on series to the FD program.

This series of experiments is called the STAR program (Sandia Transient Axial Relocation of fuel and cladding). In these experiments cinematography will be used to observe fuel and clad relocation. Multiple pin bundles (up to 8 pins) and pin lengths (including blanket) of 0.4 m will be used. Flowing gas will be used to simulate sodium vapor streaming, which will provide a driving force to relocate fuel and cladding. It is expected that material relocation velocities and the flow regimes can be determined for both clad and fuel relocation under varying heating conditions and gas flow velocities. This information will then be useful for development and verification of initiation phase fuel behavior.[19]

6.0 REFERENCES

1. D. C. Williams, et al, "LMFBR Accident Delineation Study--Phase I Final Report," SAND80-1267 (Albuquerque, NM: Sandia National Laboratories, November 1980).

2. G. L. Cano, R. W. Ostensen, M. F. Young, Visual Investigation of Reactor Fuels Response To Simulated LOF Heating Conditions, First Series, SAND79-0940 (Albuquerque, NM: Sandia National Laboratories).

3. S. A. Wright, P. K. Mast, et al, Fuel Disruption Experiments Under High Ramp Rate Heating Conditions, SAND81-0413 (Albuquerque, NM: Sandia National Laboratories).

4. S. A. Wright and P. K. Mast, "Visual Observations of Fuel Disruption in In-Pile LMFBR Accident Experiments", Proceedings of the Conference on Fast, Thermal, and Fusion Reactor Experiments, Salt Lake City, Utah, April 12-15, 1982.

5. S. A. Wright, P. K. Mast, et al, "In-Core Fuel Disruption Experiments Simulating LOF Accidents for Homogeneous and Heterogenous Core LMFBRs: FD2/4 Series," Proceedings of the International Topical Meeting on Liquid Metal Fast Breeder Reactor Safety and Related Design and Operational Aspects, Lyon, France, July 19-23 1982.

6. S. A. Wright, P. K. Mast, G. Schumacher, "LOF Accident Simulations for Homogeneous and Heterogeneous Core LMFBRs: FD2/4 Series", ANS Transactions, Washington D. C., November 14-19, 1982.

7. S. K. Rhow, D. M. Switick, et al, An Assessment of HCDA Energetics in the CRBRP Heterogeneous Reactor Core, CRBRP-GEFR-00523 (Sunnyvale, CA: General Electric, 1981).

8. P. Royl, M. Cramer, et al, "Analysis of Hypothetical Loss of Flow Accidents without Scram in the SNR-300 End of Life Mark 1A Core Using the SAS3D Code System", Proceedings of the International Meeting on Fast Reactor Safety Technology, Seattle, WA, August 19-23, 1979, p. 624.

9. J. Dadillon, et al, Cabri Program - Main Experimental Results of the First Half of the Test Program (15 Tests), CABRI Note C 403/83.

10. E. A. Fischer and S. A. Wright, "Analysis of the FD 2/4 Experiments Performed at Sandia Laboratories", presentation at the Specialist Workshop on Fission Gas Behavior in Safety Experiments, Saint Paul LezDurance, France, October 5-7, 1983.

11. J. R. Matthews and M. H. Wood, "Modeling the Transient Behaviour of Fission Gas," Journal of Nuclear Materials 84, pp. 125-136, 1979.

12. R. W. Ostensen, FISGAS--A Code for Fission-Gas Migration and Fuel Swelling in an LMFBR Accident, SAND78-1790 (Albuquerque, NM: Sandia National Laboratories, November 1979).

13. D. H. Worledge, Fuel Fragmentation by Fission Gases During Rapid Heating, SAND80-0328 (Albuquerque, NM: Sandia National Laboratories, June 1980).

14. L. Vaeth, Current Status of Modeling Fission Gas Behavior in the Karlsruhe code Langzeit/Kurzzeit, KFK-2962 (Karlsruhe, FRG).

15. D. Hull and D. E. Rimmer, Philosophy Magazine, 4, 673, 1959.

16. D. D. Slagle, Creep of UO_2 at 2500°C, HEDL-SA-1079 (Richmond, WA: Hanford Engineering Development Laboratory, 1977).

17. A. H. Cottrell, "Theory of Brittle Fracture in Steel and Similar Metals," Transactions of the AIME, 212, 192, 1958.

18. R. J. Dimelfi and L. W. Deitrich, "The Effect of Grain Boundary Fission Gas on Transient Fuel Behavior," Nuclear Technology, 43, May 1949.

19. A. M. Tentner and H. U. Wider, "Levitate - A Mechanistic Model for the Analysis of Fuel and Cladding Dynamics under LOF Conditions for SAS4A," Proceedings of the International Meeting on Fast Reactor Safety Technology, p. 2383, Seattle, WA, August 19-23, 1979.

DISTRIBUTION:

Division of Technical Information
  and Document Control
NRC Distribution Contractor
U.S. Nuclear Regulatory Commission
15700 Crabbs Branch Way
Rockville, MD 20850
  (250 copies for R7)

U.S. Nuclear Regulatory Commission (7)
Division of Accident Evaluation
Office of Nuclear Regulatory Research
Washington, DC 20555
Attn: D. F. Ross
       O. E. Bassett
       C. N. Kelber
       G. Marino
       R. T. Curtis
       R. W. Wright
       P. Wood

U.S. Nuclear Regulatory Commission
Office of Nuclear Reactor Research
Clinch River Breeder Reactor Program Office
Washington, DC   20555
Attn: C. Allen

U.S. Department of Energy
Office of Nuclear Safety Coordination
Washington, DC 20545
Attn: R. W. Barber

U.S. Department of Energy (2)
Albuquerque Operations Office
P. O. Box 5400
Albuquerque, NM 87185
Attn: J. R. Roeder, Director
          Transportation Safeguards Division
       D. L. Krenz, Director
          Energy Technologies Division
          For: C. B. Quinn
                R. N. Holton

Los Alamos National Laboratory
P. O. Box 1663
Los Alamos, NM 87145
Attn: C. R. Bell, Q-7

41

DISTRIBUTION (Continued)

Technology Management Center
Argonne National Laboratory
Building 207
9700 S. Cass Avenue
Argonne, IL 60439
Attn: L. Baker

Department of Nuclear Energy
Building 820
Brookhaven National Laboratory
Upton, NY 11973
Attn: T. Ginsberg

Argonne National Laboratory (9)
9700 South Cass Avenue
Argonne, IL 60439
Attn: B. W. Spencer
      J. J. Sienicki
      J. M. Kramer
      T. E. Kraft (3)
      G. Feuske
      L. W. Deitrich
      R. Demelfi

Dr. Carl A. Erdman
Nuclear Engineering Department
Texas A and M University
College Station, TX 77843

General Electric Corporation
310 DeGuigne Drive
Sunnyvale, CA 94086
Attn: T. I. Temme, Mgr.,
      Probabilistic Risk Assessment

Fauske and Associates, Inc.
16W070 West 83rd Street
Burr Ridge, IL 60521
Attn: Dr. Michael Grolmes

DISTRIBUTION (Continued)

Projekt Schneller Brueter (10)
Kernforschungszentrum Karlsruhe GMBH
Postfach 3640
D75 Karlsruhe
West Germany
Attn: Dr. Kessler (2)
        Dr. Heusener (2)
        Dr. Froelich
        Dr. Werle
        Dr. Kuhn
        Dr. Groetzbach
        Dr. E. A. Fischer
        Dr. Vaeth

UKAEA Safety and Reliability Directorate (4)
Wigshaw Lane
Culcheth
Warrington WA3 4NE
Cheshire
England
Attn: Mr. J. G. Collier, Director
        Mr. E. V. Gilby
        Dr. M. J. Hayns
        Dr. R. S. Peckover

AERE Harwell (2)
Didcot
Oxfordshire OX11 ORA
England
Attn: Dr. J. R. Matthews,
        Theoretical Physics Division
        Dr. J. Gittus, AETB

UKAEA (2)
Risley
Warrington WA3 6AT
Cheshire
England
Attn: Dr. B. Cowking, FRDD
        Dr. D. Hicks, TRDD

Dr. F. Briscoe
Culham Laboratory
Culham
Abingdon
Oxfordshire OX14 X
England

DISTRIBUTION (Continued)

Mr. C. P. Gratton
Division Head, SESD
Atomic Energy Establishment
Winfrith,
Dorset DTZ 8DH
England

K. S. Norwood
Mail Stop B 12
Building 4500 N
Oak Ridge National Laboratory
P. O. Box X
Oak Ridge, TN 37830

Joint Research Centre (3)
Ispra Establishment
21020 Ispra (Varese)
Italy
Attn: H. Holtbecker
        P. Fasoli-Stella
        R. Klersy

Power Reactor and Nuclear Fuel (6)
  Development Corporation (PNC)
Fast Breeder Reactor Development Project (FBR)
9-13, 1-Chome, Akasaka
Minato-Ku, Tokyo
Japan
Attn: Dr. A. Watanabe
        Dr. K. Takahashi
        Dr. N. Tanaka (3)
        Dr. N. Nonaka

Centre d'Etudes Nucleaires de Cadarache (4)
Boite Postale No. 1
13115 St. Paul lez Durance
France
Attn: A. Meyer-Heine DERS/SIES
        J. Cl. Melis DERS/SIES
        M. Schwarz DERS/SIES
        C. LeRigoleur DRNR/SYTC

DISTRIBUTION (Continued)

1230 J. E. Powell
3141 C. M. Ostrander (5)
3161 W. L. Garner
3461 B. N. Yates
6000 E. H. Beckner
6320 R. M. Jefferson
6400 A. W. Snyder
6410 J. W. Hickman
6412 A. L. Camp
6420 J. V. Walker
6420 M. Hasti
6420 M. Watkins
6421 T. R. Schmidt
6422 D. A. Powers
6422 J. E. Brockmann
6422 R. M. Elrick
6422 A. R. Taig
6423 P. S. Pickard (2)
6423 A. C. Marshall
6423 D. A. McArthur
6423 G. Schumacher
6423 S. A. Wright (5)
6425 W. J. Camp
6425 G. Kayser
6425 P. K. Mast
6425 M. F. Young
6427 J. T. Hitchcock
6440 D. A. Dahlgren
6450 J. A. Reuscher
6451 T. F. Luera
6452 M. F. Aker
6453 W. J. Whitfield
7100 C. D. Broyles
7530 T. B. Lane
     Attn: N. R. Keltner, 7537
            R. U. Acton, 7537
            T. Y. Chu, 7537
7550 T. S. Edrington
     Attn: O. J. Burchett, 7551
            J. H. Gieske, 7552
8424 M. A. Pound

2. TITLE AND SUBTITLE Fuel Disruption Mechanisms Determined In-Pile in the ACRR	**1. REPORT NUMBER** (Assigned by TIDC, add Vol. No., if any) NUREG/CR-3780 SAND83-1750 **3. LEAVE BLANK**

1. REPORT NUMBER (Assigned by TIDC, add Vol. No., if any)

NUREG/CR-3780
SAND83-1750

3. LEAVE BLANK

2. TITLE AND SUBTITLE

Fuel Disruption Mechanisms Determined
In-Pile in the ACRR

4. DATE REPORT COMPLETED

MONTH	YEAR
April	1984

5. AUTHOR(S)

S. A. Wright, div. 6420
E. A. Fischer, KfK

6. DATE REPORT ISSUED

MONTH	YEAR
September	1984

7. PERFORMING ORGANIZATION NAME AND MAILING ADDRESS (Include Zip Code)

Sandia National Laboratories
Albuquerque, NM 87185

8. PROJECT/TASK/WORK UNIT NUMBER

9. FIN OR GRANT NUMBER

A-1016

10. SPONSORING ORGANIZATION NAME AND MAILING ADDRESS (Include Zip Code)

Division of Accident Evaluation
Office of Nuclear Regulatory Research
USNRC
Washington, DC 20555

11a. TYPE OF REPORT

technical

b. PERIOD COVERED (Inclusive dates)

12. SUPPLEMENTARY NOTES

13. ABSTRACT (200 words or less)

Over thirty in-pile experiments were performed to investigate
fuel disruption behavior for LMFBR loss of flow (LOF) accidents.
These experiments reproduced the heating transients for a variety of
accidents ranging from slow LOF accidents to rapid LOF-driven-TOP
accidents. In all experiments the timing and mode of the fuel disrup-
tion were observed with a high speed camera, enabling detailed com-
parisons with a fuel pin code, SANDPIN, which models transient intra-
and inter-granular fission gas behavior to predict the macroscopic
fuel behavior, such as fission gas induced swelling and frothing,
cracking and breakup of solid fuel, and fuel vapor pressure driven
dispersal.

This report reviews the different modes of fuel disruption as
seen in the experiments and then describes the mechanism responsible
for the disruption. An analysis is presented that describes a set of
conditions specifying the mode of fuel disruption and the heating
conditions required to produce the disruption. The heating conditions
are described in terms of heating rate (K/s), temperature gradient,
and fuel temperature. A fuel disruption map is presented which plots
heating rate as a function of fuel temperature to illustrate the
different criteria for disruption. Although this approach to
describing fuel disruption oversimplifies the fission gas processes
modeled by SANDPIN, it does illustrate the criteria used to determine
which fuel disruption mechanism is dominant and on what major fission
gas parameters it depends.

14. DOCUMENT ANALYSIS – a. KEYWORDS/DESCRIPTORS

b. IDENTIFIERS/OPEN ENDED TERMS

15. AVAILABILITY STATEMENT

unlimited

16. SECURITY CLASSIFICATION

(This page)
U

(This report)
U

17. NUMBER OF PAGES

18. PRICE